



ARTICLE

Title Supersonic Condensation and Separation Characteristics of CO₂-Rich Natural Gas under Different Pressures

Yong Zheng¹, Lei Zhao¹, Yujiang Wang¹, Feng Chang¹, Weijia Dong^{2,*}, Xinying Liu², Yunfei Li², Xiaohan Zhang² and Ziyuan Zhao³

¹Engineering Management Center, Sinopec Shengli Oilfield Company, Dongying, 257000, China

²Technical Inspection Center, Sinopec Shengli Oilfield Company, Dongying, 257000, China

³Shandong Provincial Key Laboratory of Oil & Gas Storage and Transportation Safety, College of Pipeline and Civil Engineering, China University of Petroleum, Qingdao, 266580, China

*Corresponding Author: Weijia Dong. Email: dongwj77741@163.com

Received: 24 March 2022 Accepted: 07 June 2022

ABSTRACT

Supersonic separation technology is a new natural gas sweetening method for the treatment of natural gas with high CO₂ (carbon dioxide) content. The structures of the Laval nozzle and the supersonic separator were designed, and the mathematical models of supersonic condensation and swirling separation for CO₂-CH₄ mixture gas were established. The supersonic condensation characteristics of CO₂ in natural gas and the separation characteristics of condensed droplets under different inlet pressures were studied. The results show that higher inlet pressure results in a larger droplet radius and higher liquid phase mass fraction; additionally, the influence of centrifugal force is more pronounced, and the separation efficiency and removal efficiency of CO₂ are higher. When the inlet pressure is 6 and 9 MPa, the liquefaction efficiency at the Laval nozzle outlet increases from 56.90% to 79.97%, and the outlet droplet radius increases from 0.39 to 0.72 μm, and the removal efficiency is 31.25% and 54.52%, respectively. The effects of inlet pressures on the removal efficiency of the supersonic separator are complicated and are controlled by the combined effects of liquefaction capacity of the nozzle and centrifugal separation capacity of the swirl vane.

KEYWORDS

Supersonic separator; Laval nozzle; natural gas; carbon dioxide; condensation; separation

Nomenclature

C_D	drag coefficient (–)
D_T	thermophoresis coefficient (–)
d_l	droplet size (m)
d_{ij}	deformation rate tensor (–)
E	total energy (J/kg)
F	force between the droplet and the surrounding gas (N)
F_D	drag force per unit mass of particles (N)
F_O	other forces (N)
F_S	Saffman lift force
F_T	thermophoretic force (N)



J	spontaneous nucleation rate (m^3/s)
h	total enthalpy of gas (J/kg)
h_{lv}	latent heat of condensation (J/kg)
k_{eff}	effective thermal conductivity ($\text{W}/(\text{m}\cdot\text{K})$)
l_1	length of the convergent section (mm)
M	mole fraction of CO_2 (–)
m_1	droplet mass (kg)
m_v	mass of condensed liquid per unit volume per unit time ($\text{kg}/(\text{m}^3\cdot\text{s})$)
N	droplet number ($1/\text{kg}$)
p	pressure of the mixed gas (Pa)
p_{in}	inlet pressure (MPa)
Re	relative Reynolds number (–)
r_0	inlet radius of convergent section (mm)
r_{cr}	outlet radius of convergent section (throat) (mm)
r_d	droplet radius (m)
S_h	energy source term ($\text{J}/(\text{m}^3\cdot\text{s})$)
S_m	mass source term ($\text{kg}/(\text{m}^3\cdot\text{s})$)
S_u	momentum source term ($\text{kg}/(\text{m}^2\cdot\text{s}^2)$)
S_Y	humidity source term ($\text{kg}/(\text{m}^3\cdot\text{s})$)
T	temperature of mixture gas (K)
T_{in}	inlet temperature (K)
u_1	droplet velocity (m/s)
u_i	axial velocity components (m/s)
u_j	radial velocity components (m/s)
u'_i	axial velocity fluctuations (m/s)
u'_j	radial velocity fluctuations (m/s)
V_1	droplet volume (m^3)
Y	liquid phase mass fraction (–)
Y/Y_{in}	nozzle fluidization efficiency (–)

Greek Symbols

δ	Kronecker delta number (–)
η'	removal efficiency of supersonic separator (–)
η	separation efficiency (–)
μ	dynamic viscosity of the mixed gas ($(\text{N}\cdot\text{s})/\text{m}$)
ν	dynamic viscosity ($\text{Pa}\cdot\text{s}$)
ρ_1	droplet density (kg/m^3)
ρ_g	gas density (kg/m^3)
ρ_l	density of liquid phase (kg/m^3)
ρ	mixture phase density (kg/m^3)
ρ_v	density of mixed gas (kg/m^3)
τ_{eff}	effective stress tensor (–)

Subscripts

0, 1	component
i, j	x, y -axis
l	liquid phase
g	gas-phase
v	vapor phase

Abbreviations

CFD	Computational Fluid Dynamics
ICCT	Internal Consistent Classical Nucleation Theory
UDF	User Defined Function

1 Introduction

In recent years, with the optimization and upgrading of world's energy structure, natural gas has become more and more critical in the economic fields. More and more countries have proposed accelerating the pace of structural adjustments, increasing the proportion of natural gas consumption and expanding the natural gas consumption market [1–3]. Besides hydrocarbons, natural gas from wellheads often contains excessive CO₂ (carbon dioxide) and other non-hydrocarbon gases. The presence of CO₂ will reduce the natural gas calorific value and pipeline transportation capacity, and at the same time, it will cause severe corrosion of facilities and pipelines. Moreover, CO₂ can form dry ice and block the pipeline at low temperatures. Thus, CO₂ removal during natural gas processing is one of the key processes [4]. Currently, CO₂ removal methods commonly used in the industry mainly contain chemical absorption, pressure swing adsorption, physical adsorption, and membrane separation. These methods have achieved CO₂ removal to a certain extent. Still, at the same time, there are some problems such as high energy consumption, low removal efficiency, high investment cost, and large loss of hydrocarbon gas [5–7].

Supersonic separation technology is an emerging natural gas treatment technology which combines expansion refrigeration with swirling separation. In a separator, the swirling motion is generated by a swirl generation device. Natural gas expands to supersonic velocities in the Laval nozzle, resulting in low pressure and temperature. The nucleation and condensation of impure gases occur, and the impure gas begins to change into droplets. Then the liquid droplets are centrifuged onto the walls and removed from the gas mixtures. Compared with traditional processes, it has many advantages, such as being a compact structure, energy-saving, and environmentally protective innovation, of which is, widely used in natural gas dehydration [8,9] and liquefaction today [10,11].

Relevant scholars have carried out a lot of research work on the above technologies. Jassim et al. [12,13] adopted CFD technology to simulate the flow of high-pressure natural gas in Laval nozzles. They analyzed the effects of swirl strength, nozzle structure, and real gas effects on the flow characteristics. Malyshkina [14,15] used the Eulerian two-dimensional model to study the fluid flow characteristics in the supersonic separator, discussed the effects of aerodynamic shock waves on the supersonic flow field, and analyzed the influence of Mach number on the volume and composition of natural gas condensate and stress recovery ability. Ma et al. [16] developed a cone-core supersonic swirling separation device and set up an experimental platform to conduct performance tests with water and ethanol vapor as the medium. Lun et al. [17] conducted a numerical simulation study on the nonequilibrium condensation phase change law of water vapor during supersonic flow.

Shooshtari et al. [18] established a two-component condensation theoretical model based on the mass transfer rate and applied the model to the simulation calculation of supersonic condensation of water vapor. Wen et al. [19] conducted field tests using a new type of natural gas supersonic dehydration device. The results show that the energy loss can be minimized through an overall optimization design. It can also reduce the power consumption of the refrigeration compressor by 50%–70% compared with the low-temperature process of propane refrigeration under the condition of the same condensate yield. Bian et al. [20,21] proposed a theoretical model for the supersonic condensation of natural gas mixtures; the condensation process of the methane-ethane mixture can be divided into four main stages in Bian's model. This model reveals the supersonic condensation process of the mixture from a microcosmic point of view, laying a foundation for the study of the condensation of multi-component alkane mixtures. In addition, the influence of swirl on the supersonic condensation and liquefaction characteristics of natural gas was systematically studied [22].

As a supplement and improvement to the traditional natural gas purification process, Bian et al. [23,24] put forward applying the supersonic separation technology to the field of CO₂ removal in the first place. However, up to now, the complex problems of condensation and cyclone separation in the process of supersonic CO₂ removal are still well understood. In this paper, the condensation efficiency and removal efficiency of CO₂ in supersonic separators under different pressure conditions were studied, which is of great significance to improving and developing the natural gas purification process and reduce the cost of gas field development.

2 Structure Design of the Nozzle and Supersonic Separator

Laval nozzle is the key part of realizing CO₂ condensation in supersonic separator. In order to obtain a more uniform flow field, the convergent section adopts the Vitosinski curve [25,26], and the parameters are selected as follows: $r_0 = 40$ mm, $r_{cr} = 5$ mm, and $l_1 = 140$ mm; the convergent section curve satisfies the following equation:

$$m = m_{cr} = \sqrt{\frac{k}{R} \left(\frac{2}{k+1} \right)^{\frac{k+1}{k-1}} \frac{p^*}{T^*} Aq(Ma)} \quad (1)$$

For the divergent section of the nozzle, so as to predigest the design process and realize expansion and rectification at the same time, considering the characteristics of each linear comprehensively, the straight-line method is adopted to take the shape of a cone. And the line type of the divergent section satisfies the equation [27]:

$$r_2 = \frac{l_2}{\tan \frac{\varphi}{2}} + r_{cr} \quad (2)$$

In order to ensure that the airflow is evenly accelerated to the sonic speed and to prevent the sudden change of the flow area from causing instability of the airflow, a continuous and gradual curve connection is used at the nozzle throat to get a smooth transition.

The structure and location of the cyclone should meet the separation requirements, as well as coordinates with other units in the separator. The design method in the reference adopts a rotating vane structure; the thickness and the length of the vane are 0.5 and 10 mm, respectively, and the rotation angle is 90 degrees, the swirl vane is set at the rear of the divergent rectification section, 350 mm from the inlet. The lengths of each section are shown in Fig. 1.

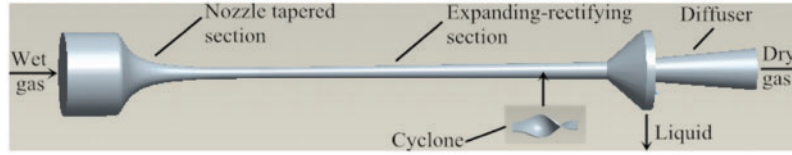


Figure 1: Structure diagram of the supersonic separator

3 Mathematical Model

3.1 Governing Equation

Based on the component transport equation of two-component fluid, the governing equations are established respectively. The gas-phase flow governing equations include mass equations, momentum equations, and energy equations. In contrast, the liquid-phase equation consists of the conservation equation for the droplet number and the relation between the parameters related to nucleating flow [28,29].

The gas-phase governing equations:

$$\frac{\partial \rho_v}{\partial t} + \frac{\partial}{\partial x_j} (\rho_v u_j) = S_m \tag{3}$$

$$\frac{\partial}{\partial t} (\rho_v u_i) + \frac{\partial}{\partial x_j} (\rho_v u_j u_i) = -\frac{\partial p_v}{\partial x_i} + \frac{\partial}{\partial x_j} \left[\mu \left(\frac{\partial u_j}{\partial x_i} + \frac{\partial u_i}{\partial x_j} - \frac{2}{3} \delta_{ij} \frac{\partial u_j}{\partial x_j} \right) \right] + \frac{\partial}{\partial x_j} (-\rho_v \overline{u'_i u'_j}) + S_u \tag{4}$$

$$\frac{\partial}{\partial t} (\rho_v E) + \frac{\partial}{\partial x_j} (\rho_v u_j E + u_j p_v) = \frac{\partial}{\partial x_j} \left(k_{\text{eff}} \frac{\partial T}{\partial x_j} + u_i \tau_{\text{eff}} \right) + S_h \tag{5}$$

$$S_m = -m_v \tag{6}$$

$$S_u = -m_v u \tag{7}$$

$$S_h = -m_v (h - h_{iv}) \tag{8}$$

The liquid-phase governing equations:

$$\frac{\partial}{\partial t} (\rho_v E) + \frac{\partial}{\partial x_j} (\rho_v u_j Y) = S_Y \tag{9}$$

$$\frac{\partial}{\partial t} (\rho_v N) + \frac{\partial}{\partial x_j} (\rho_v u_j N) = J \tag{10}$$

$$r_d = \left(\frac{3Y}{4\pi \rho_l N} \right)^{\frac{1}{3}} \tag{11}$$

3.2 Calculation Equation of Nucleation and Droplet Growth

The condensation of CO₂ gas mainly contains two processes: nucleation and droplet growth. The calculation formula of the nucleation process adopts the ICCT model. This model revised the free energy calculation formula based on previous studies. The expression form of the ICCT model has been listed in the references [30,31].

After the nucleation process is finished, the droplets begin to grow continuously. The heat transfer coefficient of a droplet in steam is in connection with the size of the droplet and the relative velocity of the droplet in the steam molecule. The growth model of droplets proposed by Gyarmathy is used to calculate the droplet growth rate [32,33].

3.3 Equations of Droplet Discrete Phase Motion

The discrete phase motion equation of a CO₂ droplet is as follows:

$$m_1 \frac{du_1}{dt} = m_1 g - \rho_g g V_1 + F \quad (12)$$

Due to the high velocity of the droplet in the swirling process, its centrifugal force far outweighs its own gravity, so the gravity term is ignored in the numerical simulation. Meanwhile, because the gas density is much less than the droplet density, the buoyancy of the droplet is ignored. The simplified discrete phase motion equation is as follows:

$$m_1 \frac{du_1}{dt} = F \quad (13)$$

$$F = F_D + F_o \quad (14)$$

The expression of F_D is as follows [34]:

$$F_D = \frac{18\mu_g C_D Re}{\rho_1 d_1^2 24} (u_g - u_1) \quad (15)$$

The other forces F_o mainly consider the effects of F_T and F_s . The expressions of these two forces are as follows [35]:

$$F_T = -D_T \frac{1}{mT} \nabla T \quad (16)$$

$$F_s = \frac{2K_k v^{1/2} \rho d_{ij}}{\rho_p d_p (d_{ik} d_{kl})^{1/4}} (u_g - u_1) \quad (17)$$

where, $K_k = 2.584$.

3.4 Meshing and Boundary Conditions

The ANSYS FLUENT 16.0 software is adopted to simulate the CO₂ supersonic condensation and separation processes. The Laval nozzle (two-dimensional) and the supersonic separator (three-dimensional) have meshed separately, and the boundary layer mesh is encrypted. In terms of the supersonic conditions, the inlet boundary and outlet conditions are set to be inlet pressure boundary and outlet pressure boundary, respectively. The time step is 10⁻⁶ in the numerical simulation. The convergence criterion is 10⁻⁶ for the energy equation and 10⁻³ for all other equations [36].

The grid independence was verified based on the above numerical calculation method. The grid numbers of the Laval nozzle and the supersonic separator were determined to be 15,410 and 281,095, respectively.

4 Results and Discussion

4.1 Condensation Efficiency of CO₂ in Laval Nozzle under Different Pressures

So as to study the CO₂ condensation in Laval nozzle under different pressure conditions, $T_{in} = 273.15$ K and $M = 0.2$ were kept unchanged. The p_{in} was set to be 6, 7, 8, and 9 MPa, respectively. The effects of inlet pressure on condensation parameters were analyzed. The variation law of condensation parameters (nucleation rate and droplet radius) under different pressure conditions was obtained by numerical simulation.

As shown in Fig. 2, it shows that when T_{in} is 273.15 K and M is 20%, as the p_{in} increases, the CO₂ condensation position moves forward. When p_{in} is 6 MPa, The condensation start position is at $x = 143.27$ mm, and when p_{in} increases to 9 MPa, the position where the condensation occurs moves forward to $x = 139.59$ mm, because the reason is when p_{in} increases, the partial pressure of CO₂ steam also increases, the greater the degree of supersaturation, the greater the degree of expansion, and spontaneous condensation is possible to occur under the same temperature. After analyzing the variation of nucleation rate and droplet radius (Figs. 2 and 3), it can be concluded that as p_{in} increases, the maximum CO₂ nucleation rate gradually decreases, and the CO₂ droplet radius gradually increases. This is because the higher the inlet pressure, the sooner the condensation occurs, the higher the temperature when condensation occurs, and the smaller the nucleation rate.

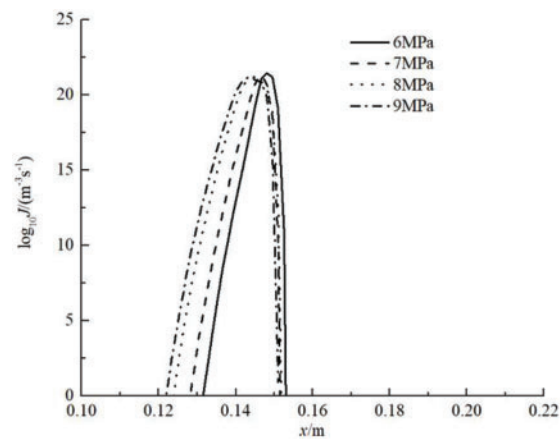


Figure 2: Nucleation rate distribution in the nozzle

So as to study the effects of p_{in} on liquefaction efficiency and droplet radius, the liquefaction efficiency at the outlet of the nozzle (the ratio of the liquid mass to CO₂ mass at the inlet) and droplet radius were calculated under different pressures; the results can be seen in Fig. 4.

As shown in Fig. 4 under the same other conditions, the CO₂ liquefaction efficiency at the nozzle outlet increases with the increase of p_{in} . As p_{in} increases from 6 to 9 MPa, the CO₂ liquefaction efficiency at the Laval nozzle outlet increases from 56.90% to 79.97%, and the outlet droplet radius increases from 0.39 to 0.72 μm . When p_{in} is smaller than 8 MPa, the increasing p_{in} has particularly obvious effects on improving the liquefaction efficiency.

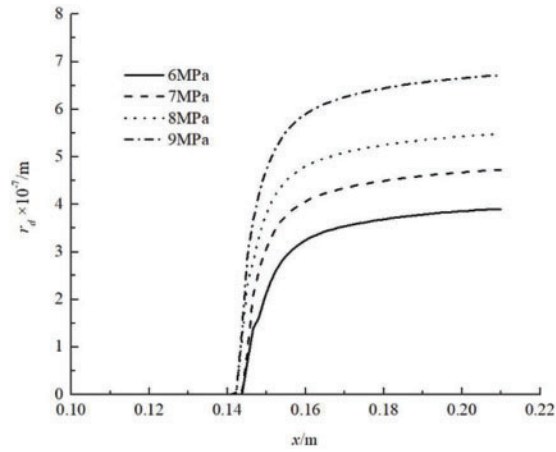


Figure 3: Droplet radius distribution in the nozzle

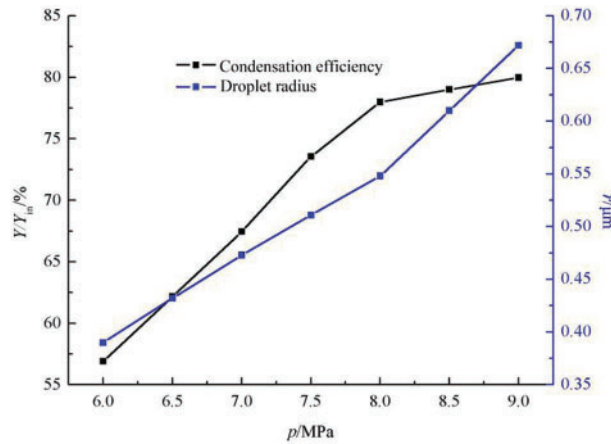


Figure 4: The effects of p_{in} on the liquefaction efficiency and droplet radius of nozzle outlet

4.2 Effects of Inlet Pressure on Separation Efficiency

After the droplets are formed, the removal of CO_2 is realized only if the separator wall captures them to form a liquid film and flow to the collector or collected directly by the sump. Therefore, in addition to the liquefaction efficiency, the separation efficiency is also an important index to evaluate if the separator structure is reasonable. During the separation process, part of the liquefied CO_2 droplets enters the collecting tank (assumed as m_{trap}). In contrast, the remaining part flows out of the dry gas outlet without separation and is re-gasified (assumed as m_{escape}). The separation efficiency η is defined as $m_{\text{trap}}/m_{\text{total}}$.

Fig. 5 shows the separation efficiency under different p_{in} conditions. It can be seen that the separation efficiency increases with the growth of the inlet pressure. When $p_{in} = 6$ MPa, the separation efficiency of the supersonic separator is only 54.92%, while p_{in} increases to 9 MPa, the supersonic separator's separation efficiency reaches 68.18%. This is because when p_{in} is smaller, the diameter of the CO_2 droplet and the centrifugal force is smaller. Most of the droplets are not captured by the wall due to the inertial effects caused by the axial velocity and are discharged with the gas. When

the diameter of the CO₂ droplet increases, the influence of centrifugal force is more apparent, and the droplet is more likely to be thrown to the wall and captured by the separator.

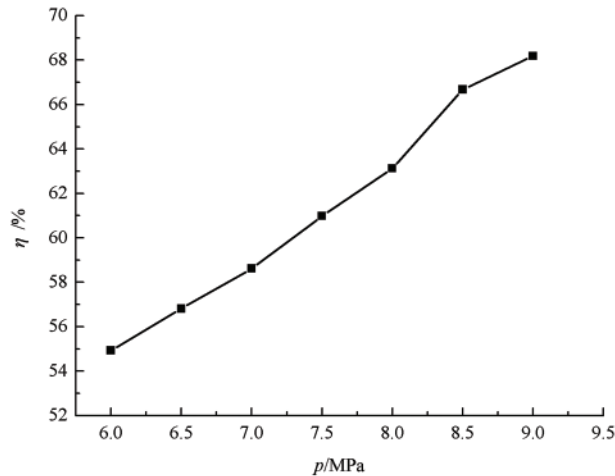


Figure 5: The effects of p_{in} on the separation efficiency

4.3 Effects of Inlet Pressure on CO₂ Removal Efficiency

The removal efficiency of CO₂ in the supersonic separation process is determined by both nozzle condensation efficiency and swirl separation efficiency. Therefore, it is necessary to evaluate the removal efficiency of the supersonic separator by comprehensively considering the two. η' is defined as Y/Y_{in} multiplied by η .

According to the liquefaction efficiency and the separation efficiency under different inlet pressure conditions obtained in the above sections, the removal efficiency of the supersonic separator under corresponding conditions is calculated, and the results are shown in Fig. 6.

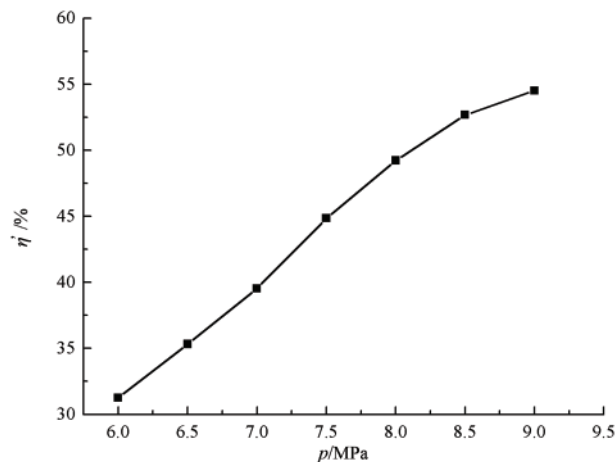


Figure 6: The effects of p_{in} on the removal efficiency

As shown in Fig. 6, the inlet pressure affects the removal efficiency obviously, and the removal efficiency increases with the growth of the p_{in} . When $p_{in} = 6$ MPa, the CO₂ removal efficiency is 31.25%,

and when p_{in} increases to 9 MPa, the CO₂ removal efficiency can be as high as 54.52%. The effects of inlet pressures on the removal efficiency of supersonic separator are mainly reflected in two aspects: one is that p_{in} affects the liquefaction efficiency of CO₂ gas; The other is that the droplet size is different when CO₂ gas condenses under different p_{in} conditions, which means that the separation efficiency of droplet after passing through the swirl vane will be different. The combined effects of the two aspects lead to significant differences in the removal efficiency of CO₂ gas under different pressure conditions.

5 Conclusions

In this paper, the supersonic condensation and swirling separation models were established. The supersonic condensation and separation characteristics of CO₂-rich natural gas under different pressures were studied. The following conclusions can be drawn:

With the increase of inlet pressure, the position of condensation moves towards the nozzle inlet, the maximum nucleation rate decreases, and the droplet radius and liquid phase mass fraction increase. The CO₂ liquefaction efficiency of the nozzle outlet increases with the growth of inlet pressure. The inlet pressure obviously affects the removal efficiency of the supersonic separator, and the removal efficiency increases with the growth of the inlet pressure.

The influence of inlet pressure on the removal efficiency of the supersonic separator is mainly reflected in two aspects: the inlet pressure affects the liquefaction efficiency of CO₂ gas. The other is that the droplet size is different when CO₂ gas condenses under different inlet pressure conditions, which means that the separation efficiency of the droplet after passing through the swirl vane will be different.

In the following research, the experimental research of supersonic condensation and separation characteristics of CO₂ under different inlet pressure conditions can be carried out to verify the numerical simulation models and results to lay a foundation for the field application of the supersonic separation technology.

Funding Statement: This work was supported by the Research Project of Technical Inspection Center of Sinopec Shengli Oilfield Company “Research of Energy Flow Optimization Analysis and Application Technology of Oilfield Production System” and the Natural Science Foundation of Shandong Province (Grant No. ZR2021QE030).

Conflicts of Interest: The authors declare that they have no conflicts of interest to report regarding the present study.

References

1. Holz, F., Richter, P. M., Egging, R. (2015). A global perspective on the future of natural gas: Resources, trade, and climate constraints. *Review of Environmental Economics & Policy*, 9(1), 85–106. DOI 10.1093/reep/reu016.
2. Scharf, H., Arnold, F., Lencz, D. (2020). Future natural gas consumption in the context of decarbonization- A meta-analysis of scenarios modeling the German energy system. *Energy Strategy Reviews*, 33, 100591. DOI 10.1016/j.esr.2020.100591.
3. Bian, J., Yang, J., Li, Y. X., Chen, Z. Q., Liang, F. C. et al. (2021). Thermodynamic and economic analysis of a novel hydrogen liquefaction process with LNG precooling and dual-pressure Brayton cycle. *Energy Conversion and Management*, 250, 114904. DOI 10.1016/j.enconman.2021.114904.

4. Faramawy, S., Zaki, T., Sakr, A. A. E. (2016). Natural gas origin, composition, and processing: A review. *Journal of Natural Gas Science and Engineering*, 34, 34–54. DOI 10.1016/j.jngse.2016.06.030.
5. Scholes, C. A., Stevens, G. W., Kentish, S. E. (2012). Membrane gas separation applications in natural gas processing. *Fuel*, 96, 15–28. DOI 10.1016/j.fuel.2011.12.074.
6. Koku, O., Perry, S., Kim, J. K. (2014). Techno-economic evaluation for the heat integration of vaporisation cold energy in natural gas processing. *Applied Energy*, 114, 250–261. DOI 10.1016/j.apenergy.2013.09.066.
7. Cao, X. W., Bian, J. (2019). Supersonic separation technology for natural gas processing: A review. *Chemical Engineering and Processing-Process Intensification*, 136, 138–151. DOI 10.1016/j.cep.2019.01.007.
8. Liu, Y., Cao, X. W., Yang, J., Li, Y. X., Bian, J. (2021). Energy separation and condensation effects in pressure energy recovery process of natural gas supersonic dehydration. *Energy Conversion and Management*, 245, 114557. DOI 10.1016/j.enconman.2021.114557.
9. Yang, Y., Walther, J. H., Yan, Y., Wen, C. (2017). CFD modeling of condensation process of water vapor in supersonic flows. *Applied Thermal Engineering*, 115, 1357–1362. DOI 10.1016/j.applthermaleng.2017.01.047.
10. Bian, J., Cao, X. W., Yang, W., Edem, M. A., Yin, P. B. et al. (2018). Supersonic liquefaction properties of natural gas in the Laval nozzle. *Energy*, 159, 706–715. DOI 10.1016/j.energy.2018.06.196.
11. Bian, J., Cao, X. W., Yang, W., Gao, S., Xiang, C. C. (2020). A new liquefaction method for natural gas by utilizing cold energy and separating power of swirl nozzle. *AIChE Journal*, 66(2), 16811. DOI 10.1002/aic.16811.
12. Jassim, E., Abdi, M. A., Muzychka, Y. (2008). Computational fluid dynamics study for flow of natural gas through high-pressure supersonic nozzles: Part 1. Real gas effects and shockwave. *Liquid Fuels Technology*, 26(15), 1757–1772.
13. Jassim, E., Abdi, M. A., Muzychka, Y. (2008). Computational fluid dynamics study for flow of natural gas through high-pressure supersonic nozzles: Part 2. Nozzle geometry and vorticity. *Liquid Fuels Technology*, 26(15), 1773–1785.
14. Malyshkina, M. M. (2008). The structure of gasdynamic flow in a supersonic separator of natural gas. *High Temperature*, 46(1), 69–76. DOI 10.1134/s10740-008-1010-5.
15. Malyshkina, M. M. (2010). The procedure for investigation of the efficiency of purification of natural gases in a supersonic separator. *High Temperature*, 48(2), 244–250. DOI 10.1134/S0018151X10020161.
16. Ma, Q. F., Hu, D. P., He, G. H., Hu, S. J., Liu, W. et al. (2009). Performance of inner-core supersonic gas separation device with droplet enlargement method. *Chinese Journal of Chemical Engineering*, 17(6), 925–933. DOI 10.1016/S1004-9541(08)60298-0.
17. Lun, Z., Chen, W., Chong, D., Liu, J., Yan, J. (2017). Numerical investigation on flow characteristic of supersonic steam jet condensed into a water pool. *International Journal of Heat and Mass Transfer*, 108, 351–361. DOI 10.1016/j.ijheatmasstransfer.2016.12.013.
18. Shoostari, S., Shahsavand, A. (2013). Reliable prediction of condensation rates for purification of natural gas via supersonic separators. *Separation & Purification Technology*, 116, 458–470. DOI 10.1016/j.seppur.2013.06.009.
19. Wen, Y., Mei, C., Huang, T., Yu, Y., Hou, J. et al. (2012). Application of supersonic separator technology in the Tarim Oil Field. *Natural Gas Industry*, 32(7), 77–79 (in Chinese).
20. Bian, J., Cao, X. W., Yang, W., Guo, D., Xiang, C. C. (2020). Prediction of supersonic condensation process of methane gas considering real gas effects. *Applied Thermal Engineering*, 164, 114508. DOI 10.1016/j.applthermaleng.2019.114508.
21. Bian, J., Cao, X. W., Yang, W., Song, X. D., Xiang, C. C. et al. (2019). Condensation characteristics of natural gas in the supersonic liquefaction process. *Energy*, 168, 99–110. DOI 10.1016/j.energy.2018.11.102.

22. Bian, J., Cao, X. W., Teng, L., Sun, Y., Gao, S. (2019). Effects of inlet parameters on the supersonic condensation and swirling characteristics of binary natural gas mixture. *Energy*, 188, 116082. DOI 10.1016/j.energy.2019.116082.
23. Bian, J., Jiang, W. M., Hou, D. Y., Liu, Y., Yang, J. (2018). Condensation characteristics of CH₄-CO₂ mixture gas in a supersonic nozzle. *Powder Technology*, 329(4), 1–11. DOI 10.1016/j.powtec.2018.01.042.
24. Cao, X. W., Guo, D., Sun, W. J., Zhang, P., Ding, G. Y. et al. (2021). Supersonic separation technology for carbon dioxide and hydrogen sulfide removal from natural gas. *Journal Clean Production*, 288, 125689. DOI 10.1016/j.jclepro.2020.125689.
25. Wang, Y., Hu, D. (2018). Structure improvements and numerical simulation of supersonic separators with diversion cone for separation and purification. *RSC Advances*, 8(19), 10228–10236. DOI 10.1039/C7RA13198D.
26. Liu, X. W., Liu, Z. L. (2017). Numerical investigation and improvement strategy of flow characteristics inside supersonic separator. *Separation Science and Technology*, 53(4), 940–952. DOI 10.1080/01496395.2017.1388256.
27. Bian, J., Jiang, W. M., Teng, L., Liu, Y., Wang, S. W. et al. (2016). Structure improvements and numerical simulation of supersonic separators. *Chemical Engineering & Processing-Process Intensification*, 110, 214–219. DOI 10.1016/j.cep.2016.10.012.
28. Wen, C., Karvounis, N., Walther, J. H., Ding, H., Yang, Y. (2020). Non-equilibrium condensation of water vapour in supersonic flows with shock waves. *International Journal of Heat and Mass Transfer*, 149, 119109. DOI 10.1016/j.ijheatmasstransfer.2019.119109.
29. Bian, J., Cao, X. W., Yang, W., Du, H., Yin, P. B. (2018). Effects of external particles on the liquefaction property of natural gas in a Laval nozzle. *Powder Technology*, 339, 894–902. DOI 10.1016/j.powtec.2018.08.077.
30. Girshick, S. L., Chiu, C. P. (1990). Kinetic nucleation theory: A new expression for the rate of homogeneous nucleation from an ideal supersaturated vapor. *Journal of Chemical Physics*, 93(2), 1273–1277. DOI 10.1063/1.459191.
31. Girshick, S. L. (1991). Comment on: “Self-consistency correction to homogeneous nucleation theory.” *Journal of Chemical Physics*, 94(1), 826–827. DOI 10.1063/1.460309.
32. Han, X., Zeng, W., Han, Z. (2019). Investigation of the comprehensive performance of turbine stator cascades with heating endwall fences. *Energy*, 174, 1188–1199. DOI 10.1016/j.energy.2019.03.038.
33. Zhang, G., Wang, F., Wang, D., Wu, T., Qin, X. et al. (2019). Numerical study of the dehumidification structure optimization based on the modified model. *Energy Conversion and Management*, 181, 159–177. DOI 10.1016/j.enconman.2018.12.001.
34. Ounis, H., Ahmadi, G., McLaughlin, J. B. (1991). Brownian diffusion of submicrometer particles in the viscous sublayer. *Journal of Colloid & Interface Science*, 143(1), 266–277. DOI 10.1016/0021-9797(91)90458-K.
35. Saffman, P. G. (1965). The lift on a small sphere in a slow shear flow. *Journal of Fluid Mechanics*, 22(2), 385–400. DOI 10.1017/S0022112065000824.
36. Wen, C., Ding, H. B., Yang, Y. (2020). Performance of steam ejector with nonequilibrium condensation for multi-effect distillation with thermal vapour compression (MED-TVC) seawater desalination system. *Desalination*, 489, 114531. DOI 10.1016/j.desal.2020.114531.